MAUSAM, 48, 4 (October 1997), 645-656

551.46.06 : 551.526.6

Mechanism of cold water regions observed in winter in the Indian Ocean

MASAHISA KUBOTA and MORIHEI KAWAGUCHI

School of Marine Science and Technology, Tokai University, Shimizu, Shizuoka, Japan 424

सार — बोरियल शीत ऋतु में अरब सागर में दो शीत समुद्री सतह तापमान (एस. एस. टी.) क्षेत्र पाए जाते हैं । एक क्षेत्र मेडागास्कर के उत्तर पूर्व में, और दूसरा अरब सागर के उत्तरी भाग में स्थित है। मासिक जलवायु विज्ञानिक समुद्री प्रेक्षणों से प्राप्त आँकड़ों का प्रयोग करते हुए इन क्षेत्रों में ठंडे जल के आने की क्रियाविधि की जाँच की गई है । मेडागास्कर के उत्तर पूर्व में पाए गए ठण्डे जल के कारण इस क्षेत्र के जल की कमी को पूरा करने के लिए एकमान अपसरण के कारण आने वाले जल पर पड़ने वाला विपरीत हवाओं का प्रभाव है। दूसरी तरफ, अरब सागर के उत्तरी भाग में एस. एस. टी. में कमी का मूल कारण लघुतरंग विकिरण में न्यूनीकरण के साथ-साथ अन्तर्निहित ऊष्मा अभिवाह में वृद्धि के कारण यहां के सकल ऊष्मा अभिवाह में उत्पन्न हुई कमी है। ये परिणाम मैक्रीएरी और कुन्डु (1989) द्वारा की गई गणितीय जाँच से प्राप्त हुए परिणामों से मिलते-जुलते है।

ABSTRACT. Two cold sea surface temperature (SST) regions are found in the Arabian Sea in boreal winter. One is located northeast of Madagascar, and another is located in a northern part of Arabian Sea. The mechanism for appearance of the cold water is investigated by using monthly climatological ocean observation data. The cold water found northeast of Madagascar is caused by upwelling owing to Ekman divergence associated with a reversal of wind direction. On the other hand, the decrease in SST in a northern part of Arabian Sea is basically caused by decrease of net heat flux associated with reduced shortwave radiation and increased latent heat flux. These results are consistent with results obtained from a numerical investigation by McCreary and Kundu (1989).

Key words — Indian Ocean, Cold SST, Heat flux, Ekman divergence.

1. Introduction

The Indian Ocean is the smallest of all oceans including the Southern Ocean and has several different features compared with other oceans. The most striking difference is the seasonal reversal of the Somali Current depending on the wind direction of the monsoon. Also the northern boundary of the Indian Ocean is located at considerably low latitudes. As a result, intermediate and deep water cannot be formed in the northern Indian Ocean. Therefore, heavy water must come from the Southern Ocean and the Mediterranean Sea including the Persian Gulf, The Red Sea, and the Australatian Mediterranean Sea (Tomczak and Godfrey 1994). Surface warm water flows into the Indian Ocean from the Pacific Ocean as the Indonesian Through Flow and return to the Atlantic Ocean in the inter-ocean exchange system of sea water (Gordon 1986). The exchange of sea water in the Indian Ocean is considered to be an essential part in the global system. The role of the Indian Ocean in the global climate system is discussed in detail and summarized by Godfrey *et al.* (1995). They demonstrated that many scientific questions about the Indian Ocean still exist and mentioned about what oceanic processes generate and maintain SST anomalies as a basic question.

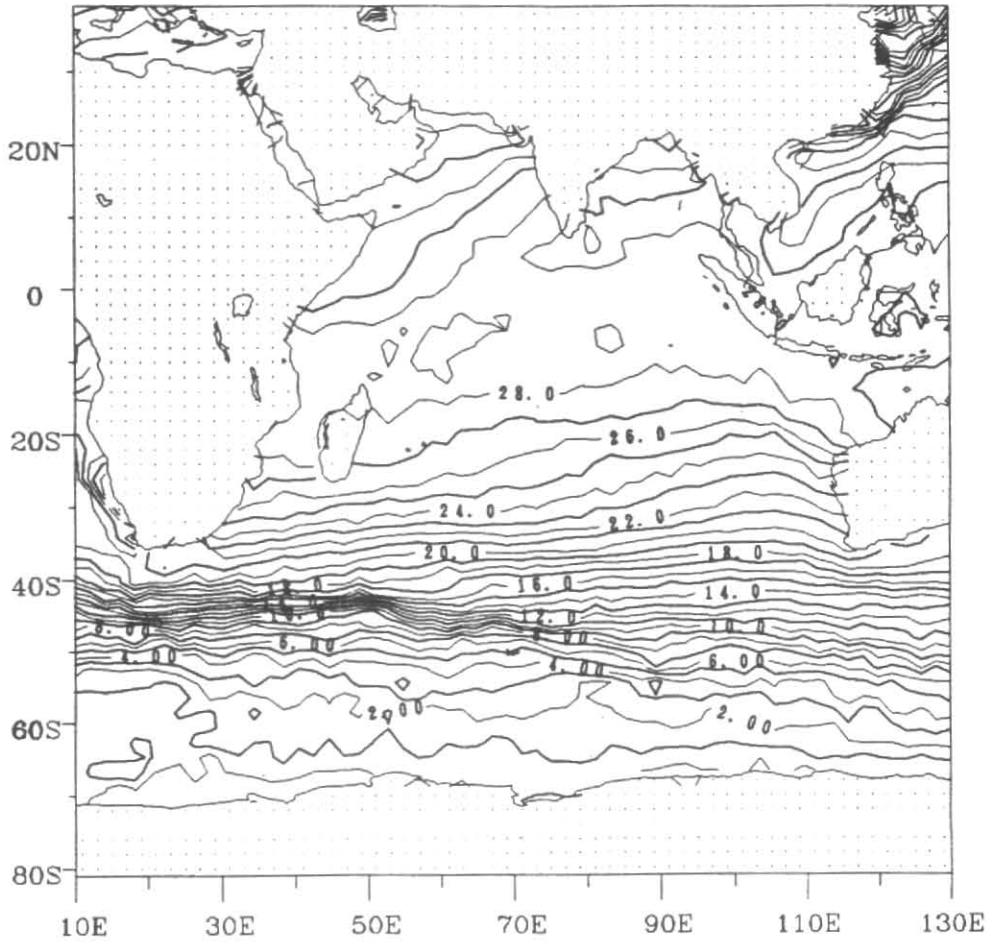

Fig. 1. SST distribution in January. The SST has a contour interval of 1.0°C

It is well known that the cool temperature region found off the Somali Coast in the summer is caused by a coastal upwelling generated by the southwest monsoon. However, there are not so many studies about the mechanism of variability of sea surface temperature (SST) in other regions. McCreary and Kundu (1989) numerically investigated SST variability in the Arabian Sea. They could succeed in simulating the observed SST patterns, generally differing by no more than 0.5°C. They demonstrated that the remarkable decrease of SST near Somalia and the Arabian peninsula during the southwest monsoon is caused by the entrainment of cool sub-surface water at the coast and its subsequent advection offshore, while that during the northeast monsoon is caused partly by reduced solar radiation and by increased evaporative cooling.

In this paper, we study SST variability in the Arabian Sea using historical ocean observation data. SST distribution in January is shown in Fig. 1. Lower SST regions are found in the northwestern region of the Arabian Basin and the northeast of the Madagascar Island. The main focus of this work is to investigate a mechanism of these lower SST regions. The data and the methods are described in sections 2 and 3 respectively. Results are given in section 4. Finally, conclusions are presented in section 5.

2. Data

In this study we have used the Monthly Summary Trimmed Group (MSTG) data in Comprehensive Ocean-Atmosphere Data Set (COADS) for 1960-92. The data for 1960-79 are in Release 1 and the data for 1980-92 are in Release 1a. MSTG data are summarized statistically for each month of each year during 1954-92, using 2° latitude $\times$ 2° longitude boxes. Many physical variables (Table 1) observed over the

TABLE 1

List of observed and derived variables (Variables, 16-19 are sensible and latent heat parameters)

(Slutz *et al.* 1985)

S.No.	Symbol	Variable
		Observed
1.	S	sea surface temperature
2.	A	air temperature
3.	W	scalar wind
4.	U	vector wind eastward component
5.	V	vector wind northward component
6.	P	sea level pressure
7.	C	total cloudiness
8.	Q	specific humidity
		Derived
9.	R	relative humidity
10.	D	$S-A$ = sea – air temperature difference
11.	E	$(S-A)W$ = sea – air temperature difference × wind magnitude
12.	F	$Qs - Q$ = (saturation Q at S) – Q
13.	G	$FW = (Qs - Q)$ W(evaporation parameter)
14.	X	WU (wind stress parameter)
15.	Y	WV (wind stress parameter)
16.	I	UA
17.	J	VA
18.	K	UQ
19.	L	VQ

ocean by ocean buoys and ships are included in COADS (Woodruff *et al.* 1987). We use some variables to be necessary for calculating each component of heat flux, for example; the wind speed(W), sea-level pressure (P), specific humidity (Q), air temperature (A), sea surface temperature(S) and total cloudiness(C). However, COADS includes many physical values derived from above-mentioned basic variables. Since most bulk formula are nonlinear, using these values derived by a sampling average seems to be more suitable than to use a monthly value of basic variables for calculating monthly heat flux. Therefore, we use the derived values, such as, $(S-A)W$ as many as possible. Also ocean observation data in the Indian Ocean are not enough to understand time variability for the various temporal scale. Therefore, we focus on the seasonal variability of SST in the Indian Ocean in the present study.

3. Method

Net heat flux between atmosphere and ocean is represented by the following equation :

$$Q_{NET} = Q_{IN} - Q_{OUT} - Q_L - Q_H \qquad (1)$$

Net heat flux consists of shortwave radiation (Q_{IN}), longwave radiation (Q_{OUT}), latent heat flux (Q_L) and sensible heat flux (Q_H). A positive value means heat transfer from atmosphere to ocean, *i.e.*, heat gain of ocean.

3.1. *Shortwave radiation* (Q_{IN})

We use Zillman (1972)'s formula for calculation of shortwave radiation following Oberhuber (1988),

$$Q_{IN} = \alpha \frac{k\gamma}{2\pi} \int_{t_1}^{t_2} \frac{S_0 \cos^2 \eta}{[(\cos \eta + 2.7)\, r.e.\, (T_A)/p + 1.085 \cos \eta + 0.1} \left(\frac{\bar{d}}{d}\right)^2 dt \qquad (2)$$

where,

$$\cos \eta = \sin \delta \sin \varphi + \cos \delta \cos \varphi \cos t$$

$$\sin \eta_{noon} = \sin \delta \sin \varphi + \cos \delta \cos \varphi$$

$$k = 1 - 0.62c + 0.0019\, \eta_{noon}$$

$$e(T_A) = 611 \times 10^{(T_A - 273.16)/(T_A - 35.86) \times 7.5}$$

$$\left(\frac{\bar{d}}{d}\right)^2 = 1.00011 + 0.00128\sin(\beta) + 0.034221\cos(\beta) + 0.000077\sin(2\beta) + 0.000719\cos(2\beta)$$

$$\delta = 0.006918 + 0.070257\sin(\beta) - 0.399912\cos(\beta) + 0.000907\sin(2\beta) - 0.006758\cos(2\beta) + 0.00148\sin(3\beta) - 0.002697\cos(3\beta)$$

t = (12 hours-solar time) $\times \pi/12$

(Parkinson and Washington 1979)

where, S_0 : Solar constant (= 1370 W/m^2)

η : Sun elevation (unit : rad)

1- γ : Albedo (= 0.06)

α : Tuning coefficient (= 0.9)

d : Actual distance between the sun and the earth

$\bar{d}$: Annual average of d

$e(T_A)$: Saturation vapour pressure in T_A

c : Cloudiness factor (In tenths)

p : Sea surface pressure

φ : latitude (rad)

t : hour angle (rad)

t_1 : Sunrise time (rad)

t_2 : Sunset time (rad)

β : Julian day (rad)

δ : declination (rad)

Since shortwave radiation exists only at the daytime, we carried out the above integration day-by-day by using the sunrise and sunset times on each day. The monthly mean value is estimated by averaging these daily values. Oberhuber (1988) reported a too strong net heat input unless a tuning coefficient is set to be 0.9. However, we basically use 1.0 as a tuning coefficient in the present study, because the theoretical reason of using the tuning coefficient is not clear. Also a too strong net heat flux is not detected in the present study even if a tuning coefficient is not set to be 0.9. The difference from Oberhuber (1988)'s results may be caused by calculating the integration on the daily basis in this study.

3.2. *Longwave radiation* (Q_{OUT})

We estimated longwave radiation by using Clark *et al.* (1974)'s following formula. This formula is based on the Berliand and Berliand (1952)'s formula with cloud correction factors given by Johnston *et al.* (1965).

$$Q_{OUT} = \varepsilon\delta T_S^4 (0.39 - 0.05 e_a^{0.5}) F(C) + 4.0\varepsilon\sigma T_s^3 (T_S - T_A) \quad (3)$$

$$e_a = E_W \times R/100 \quad (4)$$

$$\log_{10} E_W = 10.79574 (1 - T_1/T_A) - 5.02800 \log_{10} (T_A/T_1) + 1.50475 \times 10^{-4} (1 - 10^{-8.2969 (T_A/T_1)}) + 0.42873 \times 10^{-3} (10^{4.76955 (1 - T_1/T_A)} - 1) + 0.7865 \quad (5)$$

$$F(C) = 1 - bC^2 \quad (6)$$

$$b = 0.51 + 4.4 \times 10^{-3} \theta \quad (7)$$

where, T_1 : (= 273.16 °C)

T_s : Absolute temperature at sea surface (°K)

T_A : Surface air temperature (°K)

ε : emissivity of the ocean surface (= 0.97)

σ : Stefan-Boltzman constant (= 567 $\times$ 10^{-10} W/m^{2}K^4)

e_a : Vapour pressure

E_W : Saturated vapour pressure

$F(C)$: Cloud correction factors

3.3. *Latent heat flux* (Q_L), *sensible heat flux* (Q_H)

Turbulent heat fluxes, such as, latent heat flux and sensible heat flux are generally estimated by using bulk formula. In the present study latent and sensible heat fluxes are estimated by the following formulae :

$$Q_L = L \cdot \rho \cdot C_L \cdot W \cdot (Q_s - Q) \quad (8)$$

$$Q_H = C_p \cdot \rho \cdot C_H \cdot W \cdot (S - A) \quad (9)$$

$$\rho = P/[2.841(A + T_1)] \quad (10)$$

$$L = (2492.6 - 2.14 \cdot S) \times 10^3 \quad (11)$$

The bulk transfer coefficients C_L, C_H given by Kondo (1975) are adopted.

TABLE 2

Parameters in expressions for neutral bulk transfer coefficients for latent heat flux (Kondo 1975)

W (m/s)	a_L	b_L	d_L	P_L
0.3~2.2	0	1.23	0	–0.16
2.2~5.0	0.969	0.0521	0	1
5.0~8.0	1.18	0.01	0	1
8.0~25.0	1.196	0.008	–0.004	1
25.0~50.0	1.68	–0.016	0	1

TABLE 3

Parameters in expressions for neutral bulk transfer coefficients for sensible heat flux (Kondo 1975)

W (m/s)	a_H	b_H	d_H	P_H
0.3~2.2	0	1.185	0	–0.157
2.2~5.0	0.297	0.0546	0	1
5.0~8.0	1.15	0.01	0	1
8.0~25.0	1.17	0.0075	–0.00045	1
25.0~50.0	1.652	–0.017	0	1

$$10^3 C_L = a_L + b_L W p_L + d_L \ (W - 8.0)^2 \qquad (12)$$

$$10^3 C_H = a_H + b_H W p_H + d_H (W - 8.0)^2 \qquad (13)$$

where C_p : Specific heat of air

ρ : Density of air (kg/m^3)

W : Wind speed (m/s)

L : Latent heat of evaporation (J· kg)

Q : Specific humidity (g/kg)

Q_s : Saturated specific humidity at sea surface temperature (g/kg)

C_L, C_H : Bulk transfer coefficients

The dependency of constants a_i, b_i, d_i, p_i (i = L, H) on wind speeds is shown in Tables 2 and 3.

4. Results and discussion

It is well known that a remarkable cold SST region off in the Arabian Sea appears in summer. There are so many studies about the mechanism of this cold region, which show that the cool SST is caused by a coastal upwelling associated with a strong southwesterly summer monsoon. On the other hand, there are few studies about the cold SST region in winter found in the Arabian Sea (Fig. 1) except McCreary and Kundu (1989). Since the winter monsoon in the Arabian Sea is northeasterly (Fig. 2) and the wind speeds are a little bit high compared with that in spring and autumn (Fig. 3), not a coastal upwelling but a coastal downwelling can be expected to exist in winter. Therefore, we cannot explain the mechanism of the winter cold SST in the Arabian Sea by using a coastal Ekman divergence associated with the winter monsoon.

A remarkable cold tongue can be detected in boreal autumn and winter in the eastern equatorial Pacific except in El Nino year, while a cold SST region can be found northeast of Madagascar in Fig. 1. It is well-known that the cold tongue in the eastern equatorial Pacific is caused by the equatorial upwelling associated with the easterly trade wind (Philander 1990). Therefore, the cold SST region northeast of Madagascar is expected to be related to the wind system in the Indian Ocean. Wind speeds in the equatorial Indian Ocean in winter are not so high (Fig. 2). However, an interesting feature of a reversal of zonal wind direction at 10°S in the Indian Ocean is observed in Fig. 2. These features are quite different from wind system in the equatorial pacific. The reversal of zonal wind direction suggests a strong Ekman divergence and upwelling there. Therefore, the cold SST found northeast of Madagascar in winter is caused by the reversal of zonal wind direction. This is in contrast with a feature in the equatorial Pacific, caused by a combination effect by the strong trade wind and a reversal of a sign of a Coriolis parameter.

In order to confirm the mechanism of the cold SST found northeast of Madagascar in winter, we calculated Ekman flows at sea surface except an equatorial region, shown in Fig. 4. Though basically the surface Ekman flow is zonal, that in low-latitudes in the southern hemisphere is meridional and strong

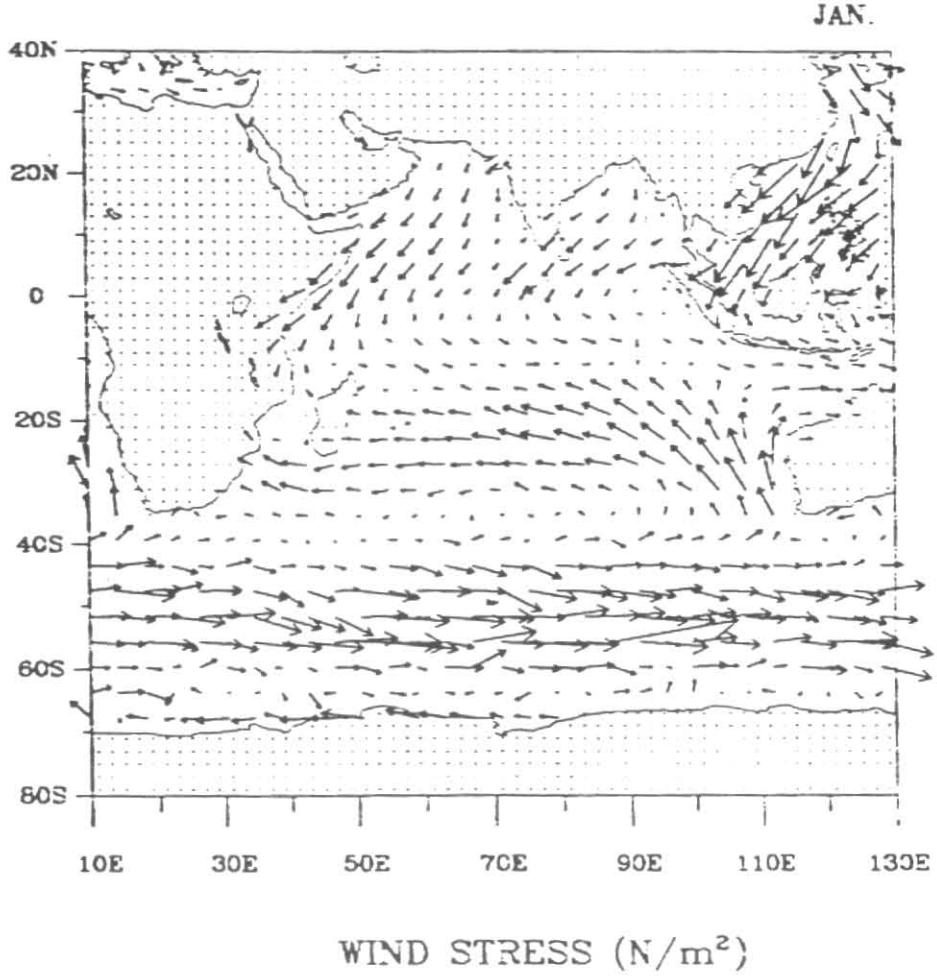

Fig. 2. Distribution of a wind stress vector in January

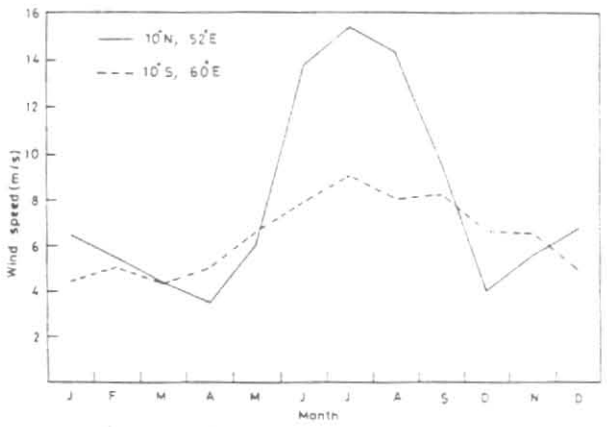

Fig. 3. Seasonal variation of wind speeds at 10°N, 52°E and 10°S, 60°E

divergence regions are found around 10°S. It should be noted that the cold SST region north of Madagascar in Fig. 1 corresponds to the region of the strong Ekman flow divergence. Therefore, it is concluded that the cause of the cold SST there in winter is the Ekman upwelling.

Generally, heat flux at sea surface is critical for the mechanism determining the SST variation. We estimated a lag cross-correlation coefficient between the monthly SST difference and the monthly net heat flux. The results are given in Fig. 5. The points with cross-correlation more than 0.5, which correspond to the 1% significance level, are shown by black dots. The respnse of SST to the heat transfer through the sea surface seems to be fairly rapid because the correlation is quite low for the results with one-month lag. The high values are located at mid-latitudes in the southern hemisphere and not found in the region corresponding to the cold region in winter. If the cause of the cold region is a dynamical effect, such as an

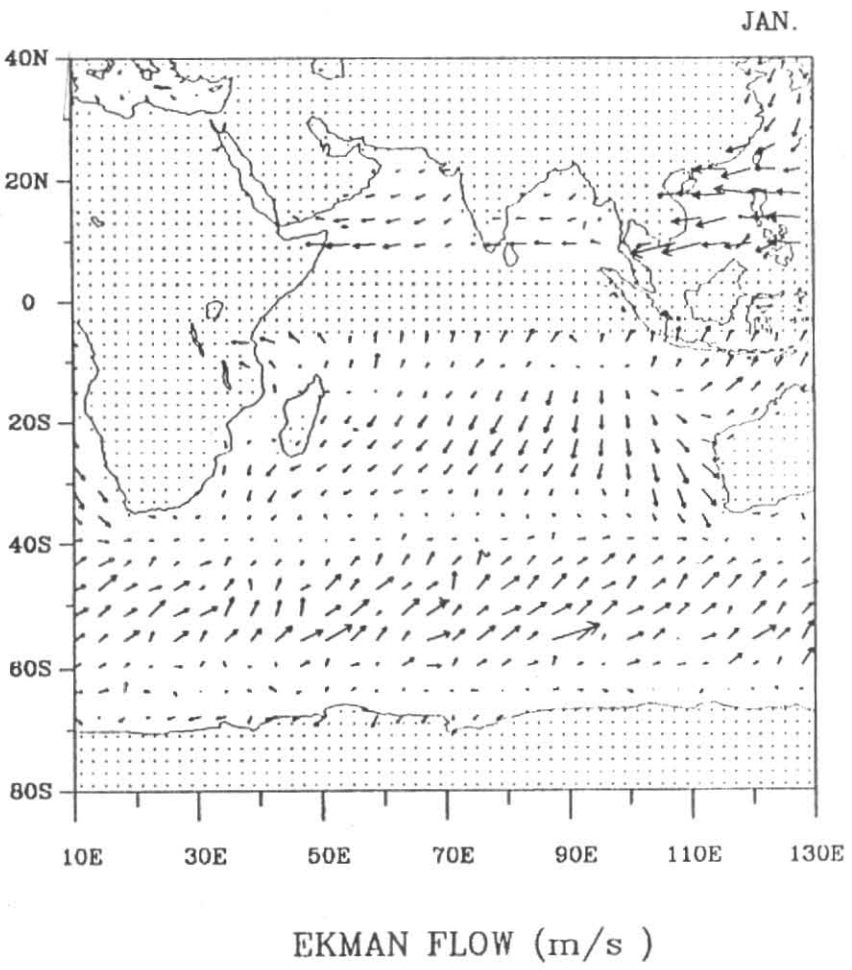

Fig. 4. Distribution of Ekman flow vectors in January

Ekman pumping, the correlation between the monthly SST difference and the monthly net heat flux should be low. Also if the cause of the cold region depends on the season, the correlation also should be low. Therefore, it is suggested that the heat flux at sea surface may not be the main mechanism for the two cold regions shown in Fig. 1. Fig. 6 shows seasonal variation of SST and net heat flux at two points in the two cold regions. Positive heat flux means heat transfer from the atmosphere to the ocean. As known, the SST variation is quite different from the net heat flux variation at 10°N, 52°E in summer because the main mechanism for the low SST in summer is not a heat transfer but a coastal upwelling related to the summer monsoon. However, the similarity of the time variation between the net heat flux and the SST is remarkable except in summer. It is concluded that the net heat flux is a dominant factor for the SST variation there except in summer. On the other hand, the variation of SST at 10°S, 60°E is not so simple compared with that of the net heat flux. The relation between the net heat flux and SST variations is not so clear, though a general feature of the annual variation is common in both variations.

Fig. 7 shows seasonal variation of net heat flux and the four components at 10°N, 52°E. The amplitudes of seasonal variation for the sensible heat flux and the longwave radiation are negligible. On the other hand, the variation of the net heat flux is anti-phase and strongly depends on that of the latent heat flux. However, the effect of the shortwave radiation on the decrease of the net heat flux in winter is not negligible. The large decrease of the net heat flux in winter is caused by the combined effect of the increase of the latent heat flux and the decrease of the shortwave radiation. Our results are quite consistent with McCreary and Kundu (1989)'s results. They investigated SST

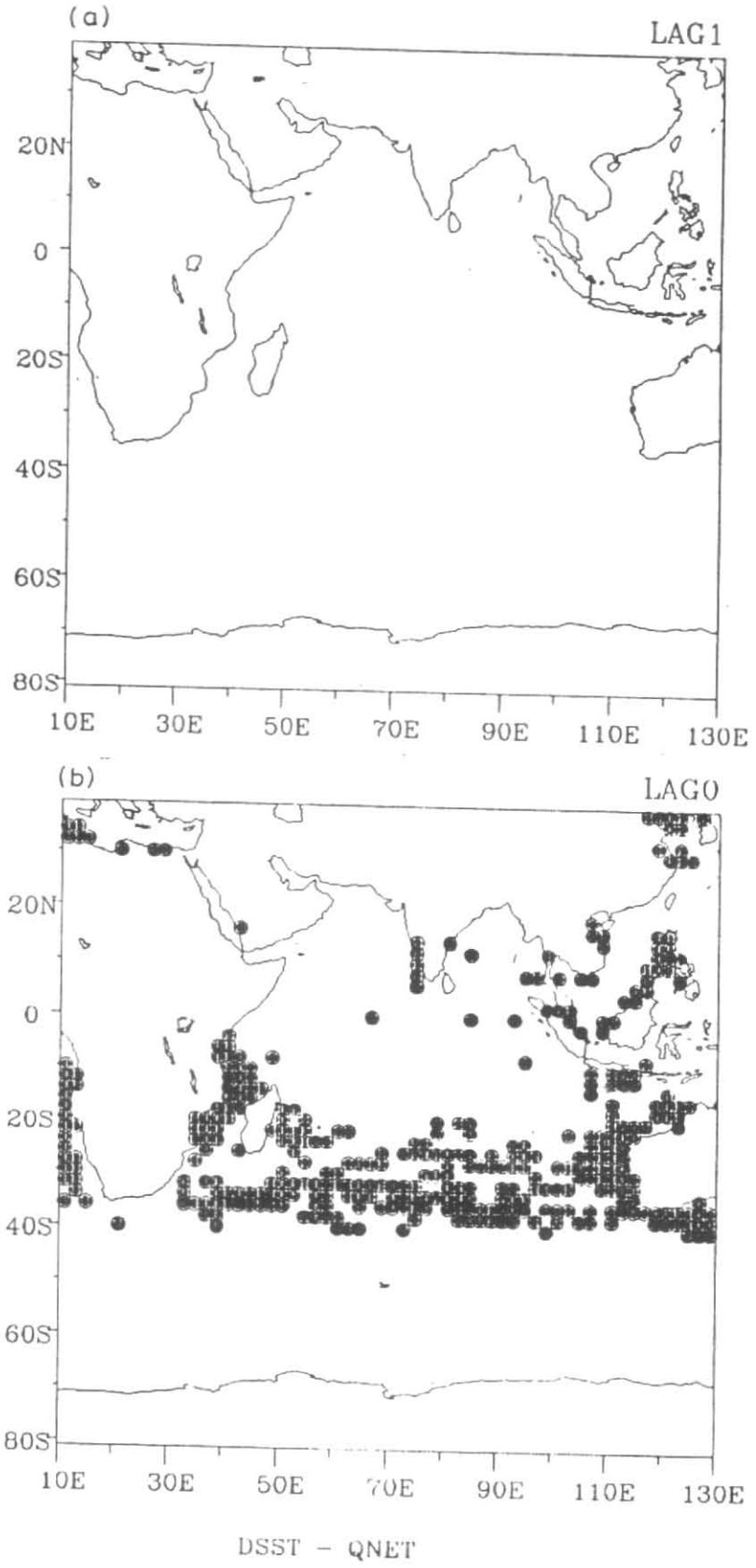

Fig. 5. High correlation areas between net heat flux and SST variation for Lag 1 and Lag 0

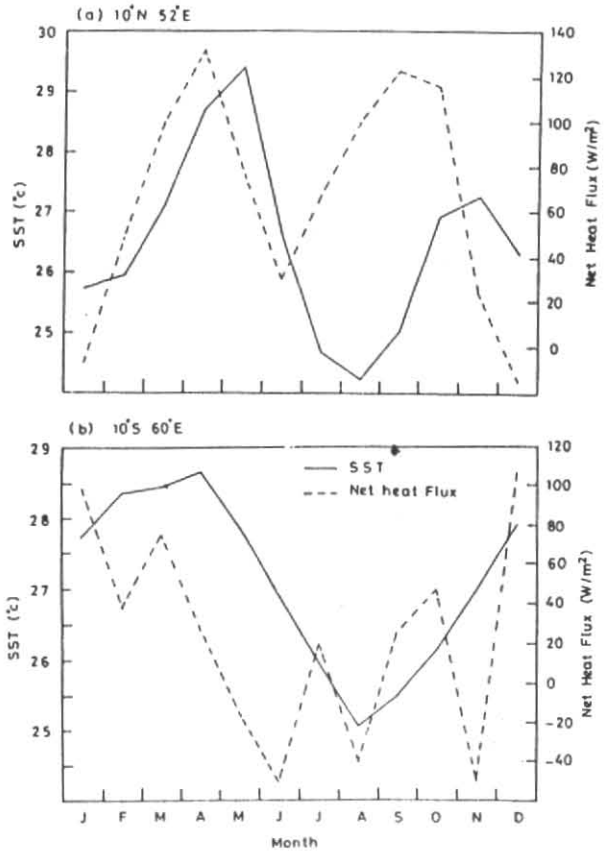

Fig. 6. Seasonal variation of SST and net heat flux at (a) 10°N, 52°E and (b) 10°S, 60°E

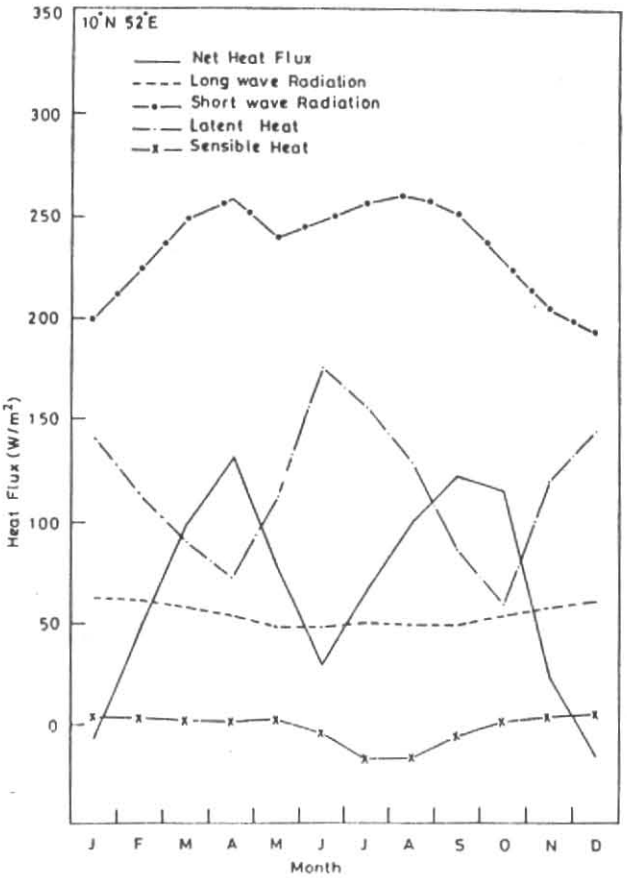

Fig. 7. Seasonal variation of each heat flux at 10°N, 52°E

variability in the Arabian Sea and concluded that during the northeast monsoon (December-March), the decrease in SST is caused in part by reduced solar radiation and by increased evaporative cooling, with additional cooling by entrainment in the northern Arabian Sea. Their conclusion obtained from their numerical investigation are also supported by the observational investigation in the present study.

The anomaly of the net heat flux in January is -73 W/m^2 of which 47% can be explained by the decrease of shortwave radiation and 33% by the increase of latent heat flux. It is concluded that the contribution by the shortwave radiation for the decrease of the net heat flux in winter is larger than that by the latent heat flux. The bulk formula for latent heat flux includes wind speed and humidity difference as a basic physical value. Fig. 8 demonstrates that the humidity difference is remarkably large and the wind speed is not so large at 10°N, 52°E in January when the SST is the minimum. Therefore, the decrease of the SST in January depends not on the wind speed but the humidity difference.

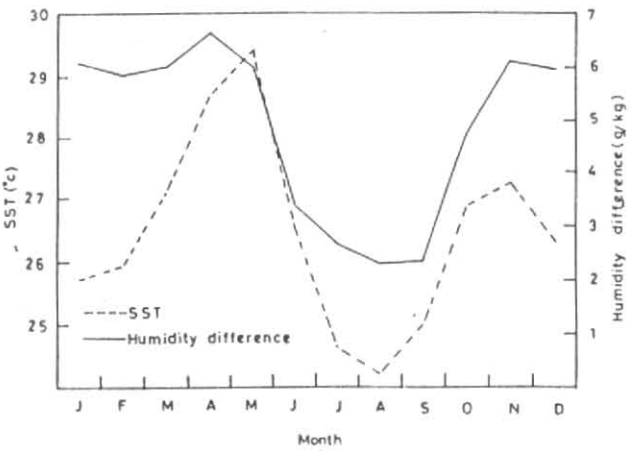

Fig. 8. Seasonal variations between SST and humidity difference

Areas of high correlation between wind speed and SST variations are shown in Fig. 9. The areas are limited in the case of 0-month lag, while the areas are larger in the case of 1-month lag. It should be noted that the high correlation areas are found in the

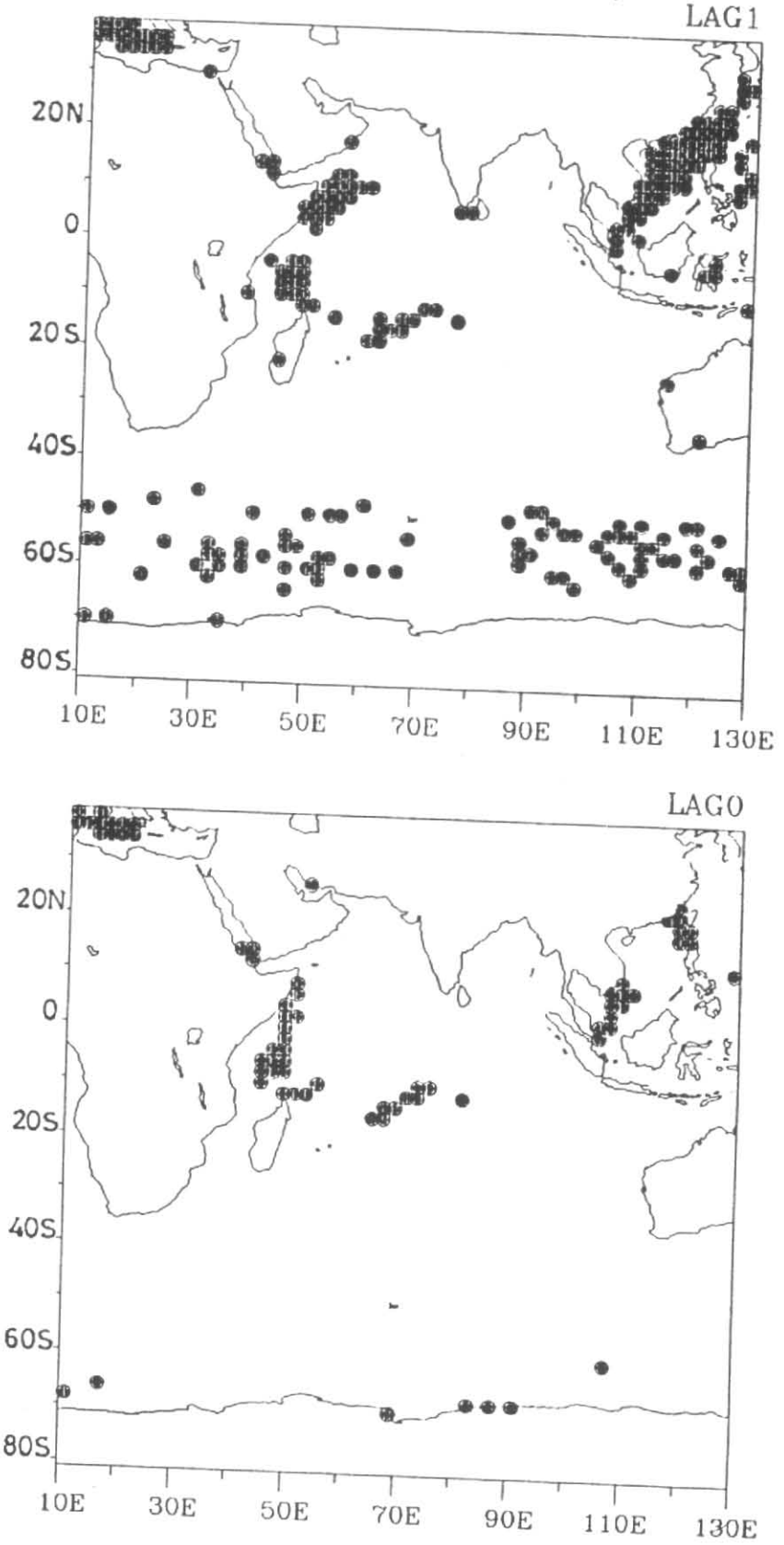

Fig. 9. Same as Fig. 5 except of SST and wind speeds

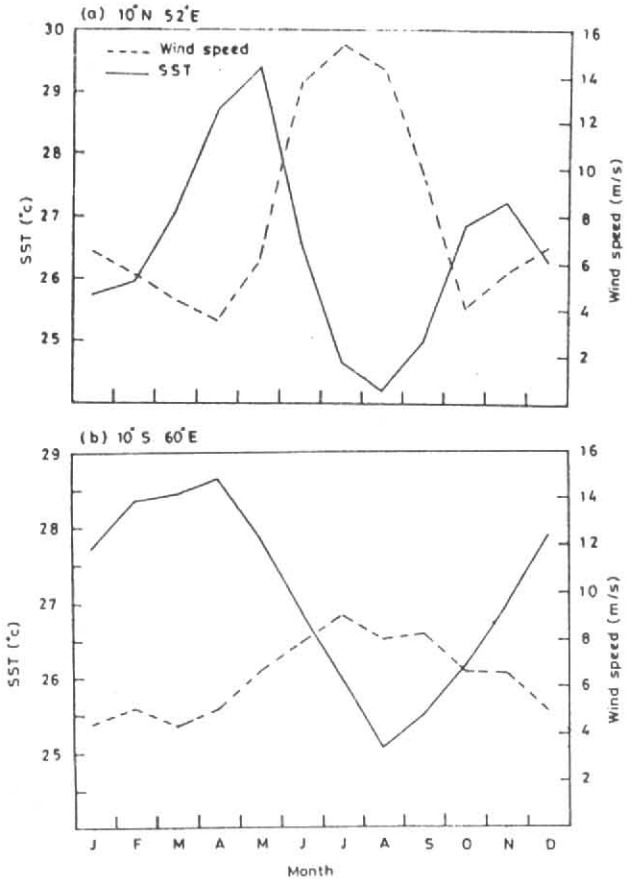

Figs. 10(a&b). Seasonal variations of SST and wind speed at (a) 10°N, 52°E and (b) 10°S, 60°E

western Arabian Sea and in the South China Sea which are located in the remarkable monsoon area. In these areas effects of the wind speed on the SST appear after one month. This feature in the Arabian Sea is also detected in Fig. 10(a) showing seasonal variations of the SST and the wind speed at 10°N, 52°E. On the other hand, the remarkable lag between the SST and the wind speed cannot be found in Fig. 10(b) showing the seasonal variation at 10°S, 60°E.

5. Conclusions

It is well known that very cool SST appears near the coasts of Arabian Sea and Somalia because of coastal upwelling caused by the strong northwest monsoon in summer. However, there are not so many studies about the SST variability in the Indian Ocean in other seasons and other areas. McCreary and Kundu (1989) developed a numerical model to study the thermodynamics of the Arabian Sea and succeeded in simulating the observed SST patterns. They showed the decrease in SST in boreal winter in the northern Arabian Sea and the decrease is caused in part by reduced solar radiation and by increased evaporative cooling. In the present study the cause of the decrease in SST in boreal winter in the northern Arabian Sea is investigated by using ocean observation data. Other cold SST regions can be found northeast of Madagascar in winter. In this study the cause of the cold water is investigated by using climatological monthly ocean observation data.

Zonal direction of the trade wind changes around 10°S in winter. As a result, a remarkable Ekman divergence and an associated upwelling can be found because the Ekman flow is meridional. This upwelling is the reason why the cold SST regions exist northeast of Madagascar in winter. The mechanism for appearance of the cold SST regions are in contrast with the cold water tongue in the eastern equatorial Pacific. The strong trade winds and the reversal of a sign of the Coriolis parameter on the equator are critical for the latter phenomenon, while the reversal of the wind direction is critical for the cold SST northeast of Madagascar.

On the other hand, considerably cold SST regions are detected in the northern Arabian Sea in winter. Since the northeast monsoon prevails in this season there, a coastal upwelling cannot be expected to be the reason of the cold SST. McCreary and Kundu (1989) demonstrated by the numerical study that during the northeast monsoon (December-March), the decrease in SST in the Arabian Sea is caused in part by reduced solar radiation and by increased evaporative cooling. Our study also indicates the decrease in SST is caused by reduced shortwave radiation and increased latent heat flux. The contribution of the former is larger than that of the latter. A bulk formulae for latent heat flux includes wind speed and humidity difference. The increase of latent heat flux there is caused by the increase of humidity difference because wind speed in winter is not so strong. The larger latent heat flux in the northern Arabian Sea in winter is pointed out by Jones *et al.* (1995), though they investigated decadal variability of surface fluxes over the Indian Ocean.

Mechanisms of appearance of the cold SST regions is investigated by using monthly climatological data. However, the data density is not so enough for this kind of investigation in the Indian Ocean. Therefore,

more detailed investigation will be carried out by using satellite data in future.

Acknowledgments

The authors would like to thank Steven Worley for providing the COADS data. Thanks are also due to Shoichi Mitsumori for his assistance. This research was partly supported by the grant-in-aid for Scientific Research on Priority Areas from the Japanese Ministry of Education, Science, Sports and Culture No. 08241111.

References

Berliand, M., Berliand, E. and Berliand, T.G., 1952, "Determination of effective radiation of the earth as influenced by cloud cover", *Izvestiia Ajd. Mauk.*, U.S.S.R., Ser. Geophyszicheskaia, No 1.

Clark, N.E., Eber, L., Laurs, R., Renner, J. and Saur, J., 1974, "Heat exchange between ocean and atmosphere in the eastern North Pacific for 1961-71", NOAA Tech. Rep. NMFS SSRF-682.

Godfrey, J.S., Alexiou, A., Ilagude, A.G., Legler, D.M., Luther, M.E., McCreary Jr., J.P., Meyers, S.R., Mizuno, K., Rao, R.R., Shetye, S.R., Toole, J.H. and Wacongne, S., 1995, "The role of the Indian Ocean in the global climate system: recommendations regarding the global ocean observing system", OOSDP Background Report Number 6, 89 p.

Gordon, A.L., 1986, "Inter-ocean exchange of thermocline water", *J. Geophys. Res.*, **91**, 5037-5046.

Jhonston, D.M., Flittner, G.A. and Cline, M.W., 1965, "Automatic data processing program for marine synoptic radio weather reports", U.S. Fish. Wildl. Serv. Spec. Sci. Rep. Fish. 503IV, 74 p.

Jones, C.S., Legler, D.M. and O'Brien, J.J., 1995, "Variability of surface fluxes over the Indian Ocean; 1960-1989, The global Atmosphere and Ocean System", **3**, 249-272.

Kondo, J., 1975, "Air-Sea bulk transfer coefficients in diabatic conditions", *Bound. Layer Meteor.*, **9**, 91-112.

McCreary and Kundu, P.K., 1989, "A numerical investigation of sea surface temperature variability in the Arabian Sea", *J. Geophys. Res.*, **94**, 16097-16114.

Oberhuber, J.M., 1988, "An atlas based on the 'COADS' data set: The budget of heat, buoyancy and turbulent kinetic energy at the surface of the global ocean", Max-Planck-Institute for Meteorology, 20 p.

Parkinson, C.L. and Washington, W.M., 1979, "A Large-scale Numerical Model of Sea Ice.", *J. Geophys. Res.*, **84**, 311-337.

Philander, S.G.H., 1990, "El Nino, La Nina and the Southern Oscillation", Academic Press, Inc., 293 p.

Slutz, R.J., Lubker, S.J., Hiscox, J.D., Woodruff, S.D., Jenne, R.L., Joseph, D.H., Steurer, P.M. and Elms, J.D., 1985, "Comprehensive Ocean-Atmosphere Data Set: Release 1. NOAA Environmental Research Laboratories", Climate Research Program, Boulder, Co., 268 p. [NTIS PB86-105723].

Tomczak, M. and Godfrey, J.S., 1994, "Regional Oceanography: An Introduction", Pergamon, 422 p.

Woodruff, S.D., Slutz, R.J., Jenne, R.L. and Steurer, P.M., 1987, "A comprehensive ocean-atmosphere data set", *Bull Amer. Meteor. Soc.*, **68**, 1239-1250.

Zillmann, J.W., 1972, "A study of some aspects of the radiation and the heat budgets of the southern hemisphere oceans", Bur. of Meteorol., Dep. of the Interior, Canberra, Australia, *Meteorol. Stud.*, **26**, 562 p.